

RESEARCH ARTICLE

10.1002/2015JD023766

Special Section:

Deep Convective Clouds and Chemistry 2012 Studies (DC3)

Key Points:

- Flash rate, energy, and channel length can be determined as moments of the flash area distribution
- Specifying channel length as a fractal helps produce stable estimates of lightning channel length
- Moments of the flash area distribution covary differently with thundercloud life cycle stage

Correspondence to:

E. C. Bruning,
eric.bruning@ttu.edu

Citation:

Bruning, E. C., and R. J. Thomas (2015), Lightning channel length and flash energy determined from moments of the flash area distribution, *J. Geophys. Res. Atmos.*, 120, 8925–8940, doi:10.1002/2015JD023766.

Received 5 JUN 2015

Accepted 10 AUG 2015

Accepted article online 13 AUG 2015

Published online 9 SEP 2015

Lightning channel length and flash energy determined from moments of the flash area distribution

Eric C. Bruning¹ and Ronald J. Thomas²

¹Department of Geosciences, Atmospheric Science Group, Texas Tech University, Lubbock, Texas, USA, ²Langmuir Laboratory for Atmospheric Research, New Mexico Institute of Mining and Technology, Socorro, New Mexico, USA

Abstract A widely used approach in observational and modeling studies of NO_x produced by lightning is to relate NO_x production to the number of flashes, without regard for the distribution of lightning flash sizes. Recent studies have begun to consider channel length and flash size, which is now observable with VHF Lightning Mapping Array data. This study uses a capacitor model for flash energy based on the flash coverage area, which defines a size scale. This flash area is then filled with channel using a fractal method and compared to other methods that estimate length directly from the VHF source locations. In the presence of instrument measurement errors, area- and fractal-based estimates are shown to be more stable estimators of flash length than connect-the-dots approaches and therefore are better suited for comparison to NO_x production. A geometric interpretation of using vertical profiles of VHF source density to weight the altitude distribution of total channel length is developed. An example of the time series of moments of the lightning flash size distribution is shown for an example case, and some meteorological interpretation is given.

1. Introduction

Fundamentally, all processes associated with a lightning flash depend on the use of electrostatic potential energy to move charge along lightning channels and the ensuing conversion of some fraction of that energy into thermal, radiative, and chemical form. One important result is the production of oxides of nitrogen (NO_x), of which lightning is the major natural source [Schumann and Huntrieser, 2007]. Both directly and as an ozone precursor, uncertainty in lightning NO_x (hereafter LNO_x) constitutes uncertainty in global atmospheric radiative forcing [Liaskos et al., 2015].

The Deep Convective Clouds and Chemistry (DC3) field campaign during the summer of 2012 was designed to better constrain the production of LNO_x across a range of climatic regimes and thunderstorm modes [Barth et al., 2015]. An important measurable in this project was the expansion of available lightning parameters from VHF Lightning Mapping Arrays (LMAs) [Rison et al., 1999; Thomas et al., 2004] for use in comparison to NO_x production measured by in situ aircraft measurements of LNO_x. A further goal of DC3 was to improve parameterizations of LNO_x production in numerical models that model the atmosphere from regional to climatic scales.

The comparison of LNO_x to lightning properties measured by LMAs depends on the accurate characterization of the lightning flash. One must account for both the geometry and driving physics of the flash itself and possible uncertainties introduced by location errors and misdetections (herein called noise sources) in the LMA data. Furthermore, a number of new lightning properties are measurable from LMA data, and their variability and sensitivity must be characterized.

Our approach here is to study the flash area and energy parameters introduced by Bruning and MacGorman [2013]. They used a simple capacitor model consistent with net charge separation by the storm's convective motions (after microphysical, collisional charging among precipitating and nonprecipitating hydrometeor species). That model was shown to be consistent with a flash energy spectrum determined by the lightning flash's area and square of the flash rate at a length scale determined from the flash's area. Flash area was determined from the convex hull A_h of the plan projection area of the VHF sources that comprised the flash. These ideas have begun to be used more widely in the DC3 analyses [Barth et al., 2015; Mecikalski et al., 2015] and have even been applied to lightning from volcanoes [Behnke and Bruning, 2015]. This study is concerned with the optimal use of the lightning measurements in such contexts and in particular the use of the distribution of

lightning flash sizes (defined by a length scale determined from their area), the length of channels associated with those flashes, and their relationship to the electrical potential energy available to each flash.

Specifically, we suspect that flash length determined from the area of the convex hull is the most stable and least affected by changes to LMA sensitivity. Therefore, in this study we examine several methods to determine the length from LMA data. In doing so, we give a geometric interpretation for the distribution of length with height based on the VHF source density. We then examine the application of these methods in one storm for illustration. We will also examine how flash length varies in time versus various flash metrics and show that it varies most closely with flash energy estimated from the capacitor model and not with the average flash length scale itself.

2. Background

The primary controls on the production of lightning NO_x remains a topic of active research. *Schumann and Huntrieser* [2007] provide a thorough review. In particular, there is debate about whether NO_x production is better correlated to the total channel length or the total energy dissipated by the flash. For example, in *Wang et al.* [1998] and *Gallardo and Cooray* [1996] the former favored flash length and the latter flash energy.

Gallardo and Cooray [1996] and *Nijdam et al.* [2010] noted uncertainty about whether the energy- NO_x relationship is linear and what part of the lightning process (high-current strokes, leaders, streamers, etc.) actually produces most of the NO_x . Likewise, *Wang et al.* [1998] studied only a single, unbranched channel and ignored the streamer/leader processes not having large currents. Other works have discussed the importance of the streamer zone in producing NO_x in sprites [*Ebert et al.*, 2006; *Nijdam et al.*, 2010]. Some of these results may also apply to tropospheric lightning. *Cooray et al.* [2009] favor NO_x production by slower non-return stroke processes (including leaders, continuing current, and recoil (K and M change) events) and that the energy associated with the return stroke is not the best measure of total production. Some recent results from observational and modeling studies support this view [*DeCaria et al.*, 2000, 2005; *Ridley et al.*, 2005; *Ott et al.*, 2010]. Finally, while some common approaches [e.g., *Price and Rind*, 1992] separate treatment of cloud and ground flash rates due to hypothesized differences in NO_x production by each flash class, *Cooray et al.* [2009] recommend the elimination of that distinction.

As *Bruning and MacGorman* [2013] noted, flash energy is related to the space (measured by area, in their study) filled by the flash; these studies point to the need to develop relationships using both flash rate and the flash geometry to relate NO_x and lightning production. In fact, the discussion of tortuosity and fractal dimension toward the end of *Wang et al.* [1998] previews the approach to be taken here, while our earlier work, expanded on in this study, touches on the energetic themes of *Gallardo and Cooray* [1996]. Due to the wide range of approaches to the NO_x production in the literature, it is clear that additional observational characterization of typical lightning channel geometry would be helpful.

For purposes of studying chemical transport, scavenging, and reactions in numerical weather prediction models, LNO_x production rate is usually parameterized on (either ground strike or total) flash rate alone [*Barthe and Barth*, 2008] and a mean NO production per flash. Flash rate is further parameterized on microphysical and kinematic characteristics of the storm. This choice of formulation of parameterizations implies that, even if flash sizes vary somewhat, they do so symmetrically about a "typical" or mean flash size, and so any underestimates due to small flashes are compensated by large ones. Furthermore, where parameterizations have been formulated against ground strike rates, the ground strike fraction for that storm is held constant. Therefore, shifts to the average flash size, skewness in the flash size distribution, and ground strike fraction would pose a problem for these parameterizations. A trend in the average flash size with time would imply a shift in the energy dissipated per flash and a change in the total channel length.

The vertical distribution of the NO_x sources also matters because of differences in transport and depletion mechanisms with height. *DeCaria et al.* [2005] and *Ott et al.* [2010] give some recent results in this area. *Hansen et al.* [2010] discussed the possibility of using the vertical profile of VHF source distributions to estimate the number of lightning channels in the vertical and thereby the vertical distribution of the NO_x source. They presented such profiles for Florida and noted that the distributions might vary in other regions of the country. Understanding such regional variability was another goal of DC3.

With the advent of LMAs, observational study of the geometric characteristics of the full lightning channel for real flashes has become possible. To date, the NASA Lightning Nitrogen Oxides Model of *Koshak et al.*,

[2010, 2014] is the most sophisticated model to make use of LMA data. It is tuned for the North Alabama Lightning Mapping Array (NALMA). They restricted their sources to $\chi^2 < 2$ and source powers of > 2 dBW to remove the influence of erroneous channel sections in their data. In *Koshak et al.* [2010], sources were averaged to a 1 km grid, which has since been refined to 100m [*Koshak and Peterson, 2011*]. At least five sources were required to participate in the location average. The averaged points were connected so that the total length was minimized. They also indicated that positive leaders do not produce enough VHF radiation to be mapped by the NALMA and that there could be an underestimate of length due to this effect. Their results are faithful to the gross channel structure of each flash but are sensitive to the detection efficiency of the network in at least two ways: location of more sources would result in more 100m grid boxes filled with at least five sources (so that tortuosity would contribute to more length), and the source power threshold aggressively eliminates the outlying extent of the channel, which they regard as erroneous. After *Koshak et al.* [2014] performed their channel length estimates, they applied a sophisticated model based on *Wang et al.* [1998] and *Cooray et al.* [2009] to account for LNO_x produced by different lightning processes. Lengths obtained by *Koshak et al.* [2010] were consistent with those obtained by *Defer et al.* [2003] [see also *Defer et al., 2001; Skamarock et al., 2003*] with an interferometer.

The goal of this paper is not to settle whether flash rate, total channel length, or dissipated energy is the most relevant quantity to NO_x production. That task is as much about the physics and chemistry of the lightning channel, which we are not able to address with our data. However, the variations in each estimation method are easily illustrated using flash extent information available from LMAs and therefore provides some additional detail about the sensitivity of such estimates that was not present in *Koshak et al.* [2014].

3. Flash Length

Because past work has cited the importance of flash length, we turn to a consideration of flash length and its relationship to flash spatial coverage and flash energy.

It has been proposed by several studies that the geometric character of lightning flashes is fractal [*Riousset et al., 2007; Vecchi et al., 1994*]. The fractal dimension D of an object describes its tortuosity and is therefore closely related to the definition of the flash length. In fact, for a purely fractal object, the length is infinite; however, the finite nature of lightning channel step lengths provides a way around this issue, as shown below.

Values of D in the literature include $4/3$ [*Tsonis, 1991*] for photos of lightning, $3/2$ for the stochastic lightning model of *Sañudo et al.* [1995], $5/3$ for the correlation dimension of LMA data [*Allen et al., 2011*], and a range from 1.6 to 1.75 for diffusion-limited aggregation processes in general [*Garik et al., 1987*]. *Niemeyer et al.* [1984] found $D = 1.7$ for their stochastic lightning model and photo of a spark.

3.1. Flash Length Estimation From Flash Spatial Coverage

For an arbitrary fractal object under study, such as a lightning flash whose VHF point sources have been recorded by an LMA, an estimate of the fractal dimension D from the box counting method [*Theiler, 1990*] is given by

$$D = -\frac{\Delta \log(n(b))}{\Delta \log(b)} = -\frac{\log(N_l) - \log(N_s)}{\log(b_l) - \log(b_s)}, \quad (1)$$

where b is the box size and N is the number of boxes covered by the object under study. Subscripts l and s refer to the large and small length scale endpoints between which a slope is taken in a log-log plot.

Consider a lightning flash composed of a cloud of points along the channel. If we choose the area of the convex hull of the plan projection of the cloud of points as our area measure A_h (it is the minimum area that spans all points without requiring a decision about the allowable degree of concavity, see also *Normant and Tricot* [1991]), we cover all points with one box. We define the scale length of this box as the square root of the area of the hull, as in *Bruning and MacGorman* [2013]. This allows us to set $N_l = 1$ and $b_l = \sqrt{A_h}$. So

$$D = \frac{\log(N_s)}{\log(\sqrt{A_h}) - \log(b_s)}. \quad (2)$$

Solving for N_s , the number of boxes at length scale b_s ,

$$N_s = \left(\frac{\sqrt{A_h}}{b_s} \right)^D. \quad (3)$$

The total length estimate L is the number of boxes multiplied by the size of the box, so

$$L = N_s b_s = b_s \left(\frac{\sqrt{A_h}}{b_s} \right)^D = \frac{(\sqrt{A_h})^D}{(b_s)^{D-1}}. \quad (4)$$

The channel step length naturally determines a lower bound on the scale at which we would expect fractal characteristics to hold and below which the channel length is a well-behaved (bounded) linear measure. This suggests that b_s should be taken to be the channel step length. Studies of channel step length [Kitagawa and Brook, 1960; Winn *et al.*, 2011; Edens *et al.*, 2014] indicate that it generally increases with height as the density of air decreases, from tens of meters near the Earth's surface to a few hundreds of meters at the tropopause. Koshak *et al.* [2015] note that the gas dynamics influencing LNO_x production depend on altitude which we do not treat here. Furthermore, the positive and negative ends appear different in optical imagery [Warner *et al.*, 2012, 2013] and laboratory studies [Williams, 2006], so there is reason to suspect differences in the proper stepping length (and dimension) to assume on each end. Nevertheless, for simplicity in this study, we assumed a single value for D and b_s for both polarities and all altitudes, though the sensitivity of the total flash length to these parameters is illustrated below.

3.2. Partitioning the Length Distribution in the Vertical

Of interest is the vertical distribution of lightning channels, which impacts the placement and transport of the NO_x source. To specify the vertical distribution, we can extend the area-based approach to channel length to a volumetric one. This method begins with a 3-D convex hull volume V_h that is calculated from a Delaunay triangulation. Each tetrahedral subvolume V_i described by the triangulation also gives the natural neighbor connectivity between the VHF sources. A modification of equation (4) gives the global, volume-based total length estimate,

$$L_3 = \frac{(\sqrt[3]{V_h})^D}{(b_s)^{D-1}}. \quad (5)$$

Assuming that the LMA detects all channel steps that matter, the tetrahedra determine a sort of natural, local step size scale related to the tetrahedral subvolumes by

$$S_i = \sqrt[3]{V_i}, \quad (6)$$

which then gives a local fractal channel length estimate of

$$L_{i0} = \sqrt[3]{\frac{V_h^D}{V_i^{D-1}}}. \quad (7)$$

By comparison with the box count methods for L and L_3 , it can be seen that the local subvolume is used in place of an assumed box size, such that the local subvolume given by the data determines the step length. Alternately, the local channel length could be determined by assuming a box size and using the volume of the local tetrahedron, which is of a form similar to L_3 :

$$P_i = \frac{(\sqrt[3]{V_i})^D}{(b_s)^{D-1}}. \quad (8)$$

Combining these equations, it is seen that the form for L_{i0} is in fact a weighting of the global, volume-based total length estimate, i.e.,

$$L_{i0} = \frac{S_i}{P_i} L_3. \quad (9)$$

Any method that makes a local length estimate should converge to the global length estimate if the latter is valid, which requires that the weighting terms S_i/P_i sum to 1. This is not in fact the case, as shown above, so a normalization factor is added and the local length estimate is

$$0L_i = \frac{S_i}{\sum_i P_i} L_3. \quad (10)$$

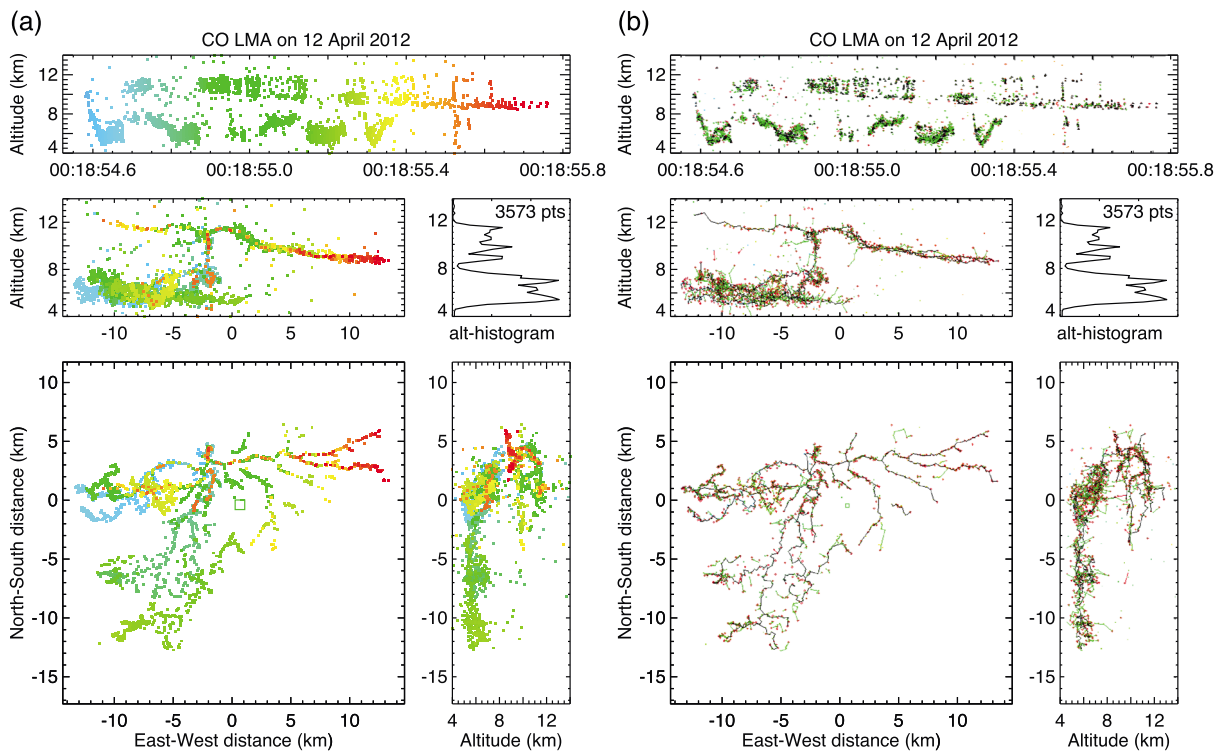


Figure 1. The flash at 0018:54 UTC on 12 April 2012. (a) Raw sources colored by time. (b) Connectivity graph showing branches (black), twigs (green) and leaves (small red diamonds.)

This formulation has the advantage that it allows the local geometry to be used to determine the local weighting of the distribution of channel length, while any length estimate can be used in place of L_3 .

Later application of equation (10) will show that the weighting method used to calculate L_i is empirically equivalent to the partition of the total channel length by VHF source density. That result might be expected, because each tetrahedron is composed of four LMA sources, and therefore the tetrahedral source density is given by $4/V_i$ (ignoring multiple counting of sources due to adjacent tetrahedra).

The geometric, space-partitioning approach to thinking about lightning channel length is helpful in diagnosing other weighting and total length methods. For instance, another weighting approach rejected during the development of equation (10) was a direct subvolume-weighted partition of the global fractal length estimate, given by $L_3 V_i / V_h$. Such an approach would have the undesirable effect of placing most of the channel length in the largest subvolumes. In the case of an H-shaped discharge in two extensive, well-separated charge layers of opposite polarity, most of the length would be assigned to the large tetrahedra that sit between the upper and lower layers, which is unphysical.

Similarly, use of L_3 has the downside that it treats the flash as isotropically propagating into the entire volume of the convex hull, while actual flashes are commonly two subsets of channels that each propagate into their respective, approximately plane-parallel potential wells. Each end of the tree is connected by a single channel, and the observed fractal branching and its associated fractal dimension are restricted to a much smaller volume of the overall volumetric hull. Therefore, use of the global length L estimated from the convex hull area in place of L_3 in equation (10) is likely more physical.

3.3. Comparison of the Fractal Length Estimate to Connect-the-Dots and Box Coverage Approaches

3.3.1. Connect-the-Dots

In order to test the flash length estimates produced by the global coverage method, it is helpful to compare to a method that directly connects each detected LMA source. Unresolved branching would lengthen the channel from this estimate. To do so, four flashes in Colorado on 12 April 2012 between 0018 and 0019 UTC were investigated in detail. We chose this interval because it had several flashes of varying size directly over the network, where sensitivity to the lowest-power VHF sources would be maximized and positional errors minimized.

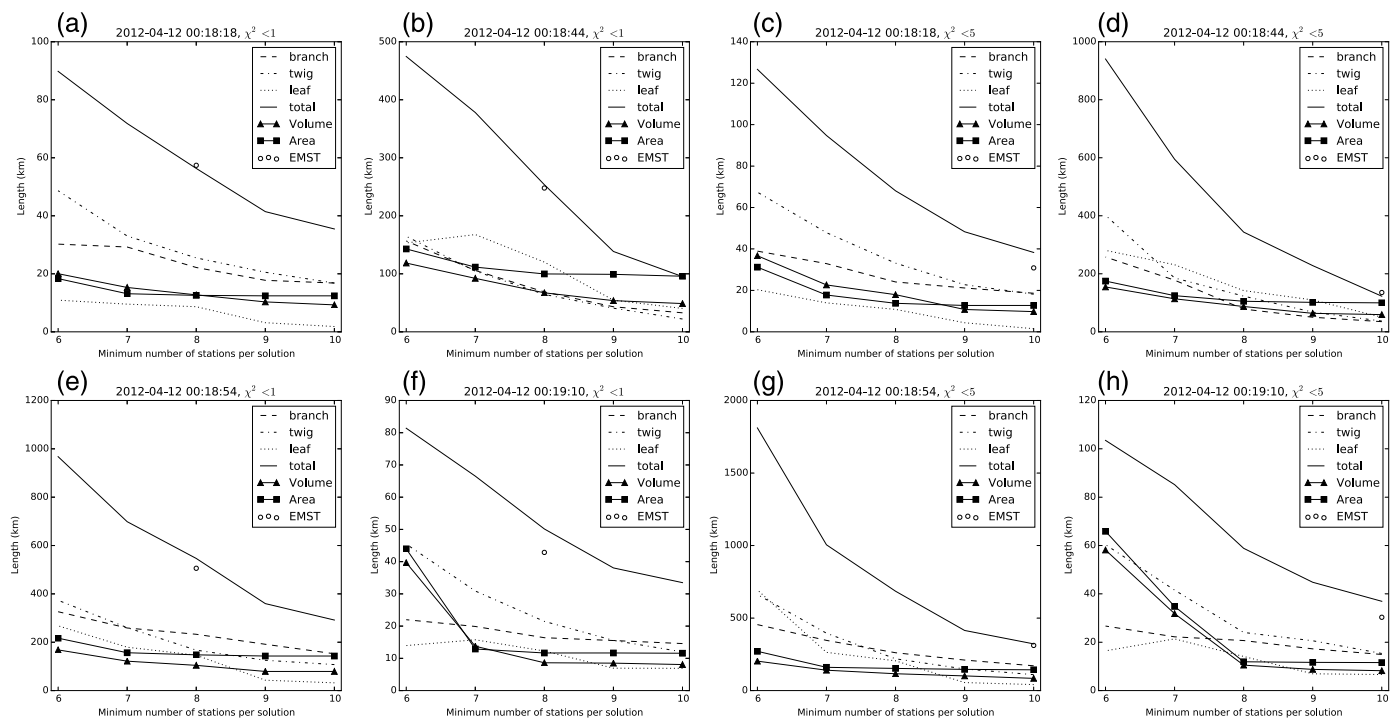


Figure 2. Sensitivity of flash length counts to number of stations using the lightning graph method (branches, twigs, leaves, and total) and the fractal method (based on convex hull areas and volumes). Each panel is for one flash; four flashes are shown and are grouped by the χ^2 threshold. The χ^2 thresholds of (a, b, e, and f) 1 and (c, d, g, and h) 5 indicated on the plot correspond to χ^2 in the data file; actual χ^2 after correcting for the observed RMS timing error of 30ns gives 5.4 and 27.2, respectively.

The flash at 0018:54 UTC illustrated the data quality achievable over the network. (Specific examples given for this flash used a minimum of eight stations and $\chi^2 < 5.0$.) Both ends of the flash were well-resolved, with the upward moving positive leaders and downward moving negative leaders (Figure 1a). All branches were very well located in plan projection. There are some points that were mislocated in height; these represent noise that should be ignored.

Our example flash shows that low-power sources are well-located by the sensitive Colorado network, to well below 0dBW, and that high-power sources are just as likely to be mislocated in the vertical as low-power sources. The greater sensitivity of the Colorado network, as well as the spatial precision provided by the network's large extent and large number of stations, allows for retention of many more sources along the channel, thereby both constraining (along the width of the channel) and extending the tortuous propagation path.

A tree-like graph (composed of nodes at source points and edges connecting those points) was constructed by connecting the nearest neighbors. The temporal sequence of development was not considered because the total amount of channel formed is the measure of interest. Each segment of the graph was classified as either a branch, twig, or leaf (Figure 1b). The connected points were classified as *branches* except at the far end of the graph. Twigs were those graph segments with fewer than 10 points after a branching node. Leaves were the end points of the graph, and if there was one point at a branching, it was classified as a leaf, not a twig. Points more than 1km from the nearest neighbor were excluded, but other points with positional errors were included in the total length estimate. The human analyst was therefore responsible for reducing the data to a single flash and controlled the presence of noise by filtering on the quality measures described next. For the data set used in this study, flashes were easily discriminated because they were widely separated in space and time.

Each VHF source location carries with it two quality measures: the number of stations N_d participating in the retrieval (higher is better) and the χ^2 goodness-of-fit statistic for the predicted arrival times [Thomas et al., 2004]. These thresholds were varied ($\chi^2 \in \{1, 5\}$; minimum $N_d \in \{6 \dots 10\}$) in order to test the sensitivity of the length retrievals to mislocated points. More restrictive quality measures removed points, which also provided a way of simulating how less sensitive networks might resolve flashes in a more sparse manner.

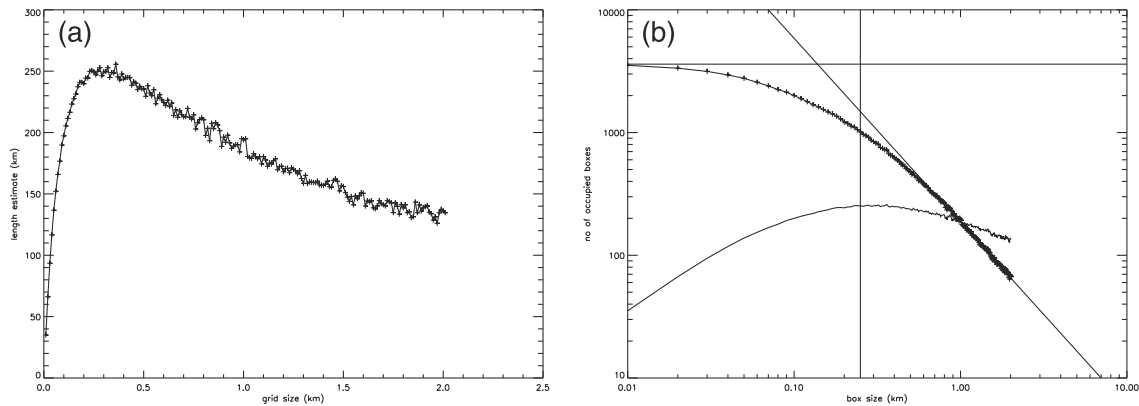


Figure 3. Length determined by box coverage for varying box sizes. (a) Length on a linear plot with peak near 250m. (b) Lower curve shows length on a log-log scale with a reference line at the box size (250m) associated with the peak. Upper curve shows the number of occupied boxes at each grid box size. Other reference lines are the total number of sources in the flash and a $D = 1.5$ power law.

Figure 2 shows the sensitivity of the lightning graph algorithm lengths to χ^2 and N_d . For all flashes and both values of χ^2 , the branches, twigs, leaves, and total lengths show a decreasing trend with an increasing minimum N_d . While there is a rapid decrease from the very large lengths for six-station solutions, there is no obvious flattening of the trend for choices of higher numbers of stations. Lengths were also estimated from the fractal method (L and L_3 for $D = 1.5$ and $b_s = 250$ m), which illustrates the sensitivity of the convex hull calculation to solution quality. Above eight stations, L was a very stable estimate and was always near the value of the main branch length from the lightning graph. On the other hand, the graph-based lengths, even for the main branch, continued to decline as the number of required stations increased. L_3 is more variable because of the inclusion of points with large altitude errors that led to a high bias in volumes at lower numbers of stations. As will be shown later, L and L_3 have a strong dependence on the fractal parameters.

The graph construction method described above is similar to that of a euclidean minimum spanning tree (EMST). For comparison, we implemented the EMST algorithm described in Ivezic et al. [2014, p. 275 and Plate 4]. Figure 2 shows a comparison of EMST lengths to total length from this study's method for eight stations at $\chi^2 = 1$ and for 10 stations at $\chi^2 = 5$. The two methods are close to one another, indicating that our graph construction method for total length is comparable to the EMST length.

3.3.2. Box Coverage

The estimated flash length for the flash at 0018:54 was also calculated by the box coverage approach using equation (4). Figure 3a shows the estimate for the entire flash for a range of grid sizes. The estimate changed with grid size. For very small cells, each cell has just one point and the estimate increases with the multiplying factor of the cell width. As the cells get too big the estimate decreases since the cell will contain points from different branches. The peak of 250km length at a box size of 250m represents the maximum number of distinct steps resolved by the LMA and so indicates a natural step length scale. For this flash, the peak length estimate from box coverage was very close to the 259km main branch length determined from the graph method.

Figure 3b shows the change in the box count and the length estimate on a log-log scale for the complete flash. The slope of the box count line at larger scales matches a reference line for the fractal dimension D of 1.5.

Table 1. Channel Length (km) From the 2-D Hull Area Given by Equation (4) for Various Values of Assumed Step Length (Box Size b_s) and Fractal Dimension D

Dimension	Step Length (m)				
	10	100	250	300	500
1.50	720	228	144	132	101
1.67	2500	538	292	259	184
1.70	3200	639	336	296	207

Table 2. Channel Length (km) From the 3-D Hull Area Given by Equation (5) for Various Values of Assumed Step Length (Box Size b_s) and Fractal Dimension D

Dimension	Step Length (m)				
	10	100	250	300	500
1.50	506	160	101	92	72
1.67	1690	363	197	175	124
1.70	2140	428	225	198	138

3.3.3. Fractal Length Estimates

While the preceding analysis suggested $D = 1.5$ and $b_s = 250$ m were appropriate choices, the discussion at the beginning of section 3 noted some variability for claims of D and b_s in earlier studies. The impact of this variability was assessed by checking the variation in length estimates with variations in D and b_s for both the two-dimensional and three-dimensional convex hulls.

Tables 1 and 2 give the channel lengths estimated from the convex hull areas and volumes of the flash at 0018:54, respectively. The results illustrate that the power law relationship results in sensitivity to D and b_s which spans a wide range. Box sizes on the order of 100–300m match best with the box coverage and connect-the-dots methods adding confidence to the importance of those length scales. The sensitivity to the fractal dimension (i.e., the tortuosity) is a factor of about 2–3, spanning the range of values given by the different lightning graph construction methods and by the different solution quality thresholds in Figure 2.

Choosing $D = 1.5$ and $b_s = 250$ m and applying equation (10) resulted in a vertical partitioning of the total flash length estimate for this flash, where the total channel length (101km, Table 2) is a global estimate from the volume of the three-dimensional convex hull. Figure 4 shows that total channel length calculated from the subvolume partitioning is equivalent to the altitude histogram of VHF sources. Note that choosing to use the area of the 2-D convex hull as the basis for the total length would increase the total length to 144km, but the same result holds; the total length at each height is increased in linear proportion.

This result illustrates the geometric basis for using the vertical histogram of VHF sources to weight NO_x production, as was done by Hansen et al. [2010].

3.4. Summary

Diagnosis of the actual channel length from the VHF measurements depends on several factors. First, the actual tortuosity of the channel may contribute an unexpectedly large amount of length. For a true fractal the length tends to infinity though the limit imposed by step length provides an upper limit in our model of lightning. By this reasoning, perhaps unintuitive channel lengths might be obtained. Second, there are

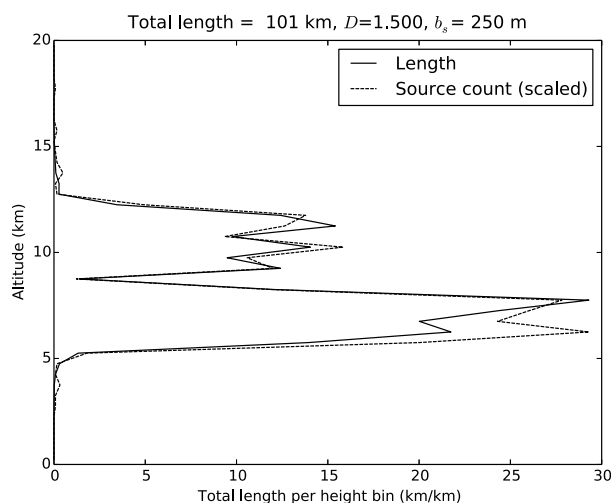


Figure 4. Vertical distribution of channel lengths and source counts using equation (10) for the flash at 0018:54 UTC on 12 April 2012. The source counts have been scaled to the same maximum as the length in each height bin.

instrument measurement errors in the location of VHF sources produced by the channel. In the best case, these are tens of meters and worse when fewer stations contribute or when χ^2 is larger [Thomas et al., 2004]. Consider the case of a non-tortuous straight line segment that has been located by a VHF mapping system. The scatter of these points would produce false additional length when all locations were connected. Such errors would be worse as more points were located at lower quality thresholds, especially because these points would also have a greater degree of statistical noise. Third, it is possible that the LMA locates nonlightning VHF sources that are falsely located near the channel and incorporated into it.

For the connect-the-dots approach, our view is that increasing quality thresholds

first remove the false locations, then noisier lightning emissions, and finally actual tortuosity. However, these sources of error are difficult to distinguish, as their occurrence overlaps to varying degrees at each quality threshold. The advantage of the convex hull approach is that it seems possible to conclusively remove all false sources and the worst mislocated real lightning sources. This is seen in the stability of the area or volume at some quality threshold. Our interpretation is that, for the Colorado network, eight stations is the threshold at which outlier-type noise is less of a factor in the connect-the-dots length, which then continues to decrease because detail is being removed from the flash. The convex hull also eliminates the need to deal with discriminating between tortuosity and instrument measurement error, because we specify the allowable tortuosity directly. However, it is still possible with the convex hull approach to get very large lengths, on the order of 10^6 m, depending on the choice of step length b_s and fractal dimension D . In our case, the graph of the main branches suggests a minimum length, though the equal-magnitude contributions from the twigs and leaves suggest that the main branch length may still be off by a factor of 2.

Estimation of the total channel length using an assumed fractal dimension and step length can be summarized as a two-step approach. Total length is estimated from whole-flash properties D , A_h , or V_h , and b_s . While estimation of the convex hull (area or volume) depends somewhat on the LMA's performance, these properties are much less sensitive to network characteristics and range from the network center than methods that use each of the sources individually. Once a total length estimate has been determined from these global properties, then it is possible to distribute the total length at the subflash level. Weighting the total length by the volume of natural neighbor tetrahedra gave a vertical channel distribution that varied like the VHF source density histogram. However, and importantly, the total flash length, including tortuosity not revealed by the LMA, can still be captured, because of the use of a fractal parameterization of the space-filling nature of the flash. This point is especially applicable at longer ranges or for less sensitive networks, where the tortuosity is fundamentally undersampled and instrument measurement errors dominate.

Because of the power law functional form, the variability in total flash length is highly sensitive to D and b_s . These parameters represent geometric characteristics that relate closely to the physics of the flash development (diffusion-limited charge transport to the extending channel and leader step length, respectively), and so effort spent in the future optimizing the choice of these parameters also constitutes an important test of our understanding of lightning physics. As noted above, our choice of $D = 1.5$ and $b_s = 250$ m is consistent with the box coverage method, past literature, and physical expectations for step length at typical flash altitudes, so we recommend those values as a starting point.

4. Illustration of Flash Length and Other Flash Statistics in a DC3 Storm

As part of the DC3 data processing, VHF source data were clustered into flashes using the *McCaul et al.* [2009] algorithm, using all points with $\chi^2 < 1$ and detected by at least seven stations. Each flash consisted of points within 3 km and 0.15 s of one another. The results of this flash clustering were used to examine the flash size statistics for a storm on 22 June 2012 from 22 to 00 UTC. This storm was targeted for aircraft observations during DC3, as described by *Barth et al.* [2015]. In this section we investigate the size statistics for this storm in detail, looking in particular at the total energy and flash length characteristics.

Figure 5 shows the flash rate, total energy, and first four moments of the flash size distribution (mean, standard deviation, skewness, and kurtosis) from all flashes belonging to that thunderstorm cell. Details of these calculations are provided in Appendices A–C. The storm produced lightning flashes for about an hour and a half.

The storm's first flashes occurred at 2050 UTC. Flash rates increased until 2108 UTC, after which they decreased from 19 fl min^{-1} (flashes per minute) to $9\text{--}10 \text{ fl min}^{-1}$ between 2124 and 2130 UTC. Flash rates then increased to a maximum of 26 fl min^{-1} at 2142 UTC, before falling rapidly to 4 fl min^{-1} by 2152 UTC and remaining at $1\text{--}2 \text{ fl min}^{-1}$ after 2200 UTC. Lightning ceased by 2224 UTC.

Mean flash size and, to a lesser extent, the standard deviation of flash size tended to peak when flash rates were small, and vice versa, as predicted by *Bruning and MacGorman* [2013] and recently confirmed in Alabama storms by *Mecikalski et al.* [2015] and for other DC3 storms by *Barth et al.* [2015]. Flash sizes increased from the time of first flash until 2124 UTC (at the local minimum in flash rate), when the mean flash size was 10 km. (Note that this size is roughly the width of the flash, i.e. $l = \sqrt{A_h}$ as defined in Appendix A, which is different from the tortuous channel length L .) Thereafter the mean size scale decreased to 5 km during the maximum in

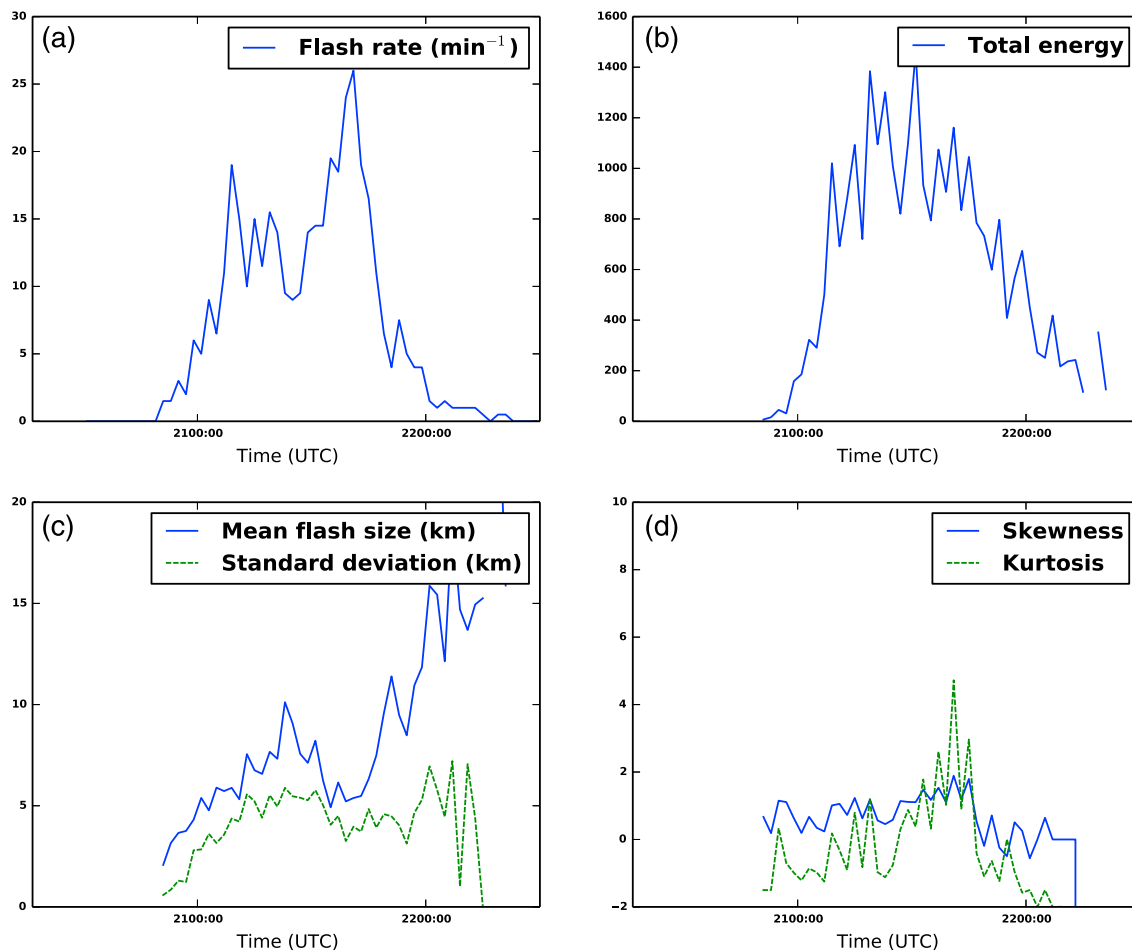


Figure 5. Time series of flash size statistics from a storm in Colorado on 22 June 2012 (DC3 IOP21a) between 2050 and 2230 UTC. (a) Flash rate (per minute), (b) total flash energy dissipation rate per unit K ($\text{Js}^2 \text{kg}^{-1} \text{min}^{-1}$), (c) mean flash size (km, solid line) and standard deviation of flash size (km, dashed line), and (d) skewness (solid line) and kurtosis (dashed line) of the flash size distribution.

flash rate at 2140 UTC. Flash sizes were large for the rest of storm: generally about 15km during the last 20min of flashing.

Flash energy did not have obvious maxima at the same times that flash rates were large. After the initial maximum in flash rate was attained, total energy continued to increase, remaining at broad maximum with fluctuation between 800 and 1400 from 2110 to 2145 UTC. Energy decreased thereafter; while flash rates were 1–2 per minute after 2200 UTC, total energy remained at 200 because those flashes were large. While the higher-order skewness and kurtosis statistics (Figure 5d) were noisy, the size distribution exhibited nonzero skewness.

The temporal evolution in flash trends may be useful as an indicator of the stage in storm life cycle, as suggested by *Bruning et al.* [2007] in their study of lightning observations relative to the life cycle of a small multicellular storm. This storm's trends were divided into roughly three intervals. As the storm became established, flashes were small initially, with the average size scale increasing to about 5–6km until the first maximum in flash rate at 2105 UTC. A modulation period then began. As flash rates decreased from the first peak, the average flash size scale increased to barely 10km by 2120 UTC. Thereafter, another increase in flash rate took place, and the average flash size scale decreased once again to about 5km by 2140 UTC. Thereafter, the decay of the storm began. Flash sizes steadily increased as flash rates plummeted; the average flash size scale exceeded 10km after about 2150 UTC. Trends in energy offer an additional view of the storm's life cycle. Energy increased as the storm became established through 2105 UTC. Active updrafts presumably dominated the volume of the storm during this period. Energy then fluctuated at its highest levels, with little discernible trend: during the modulation stage, flash size and rate compensated for one another. During the decay stage,

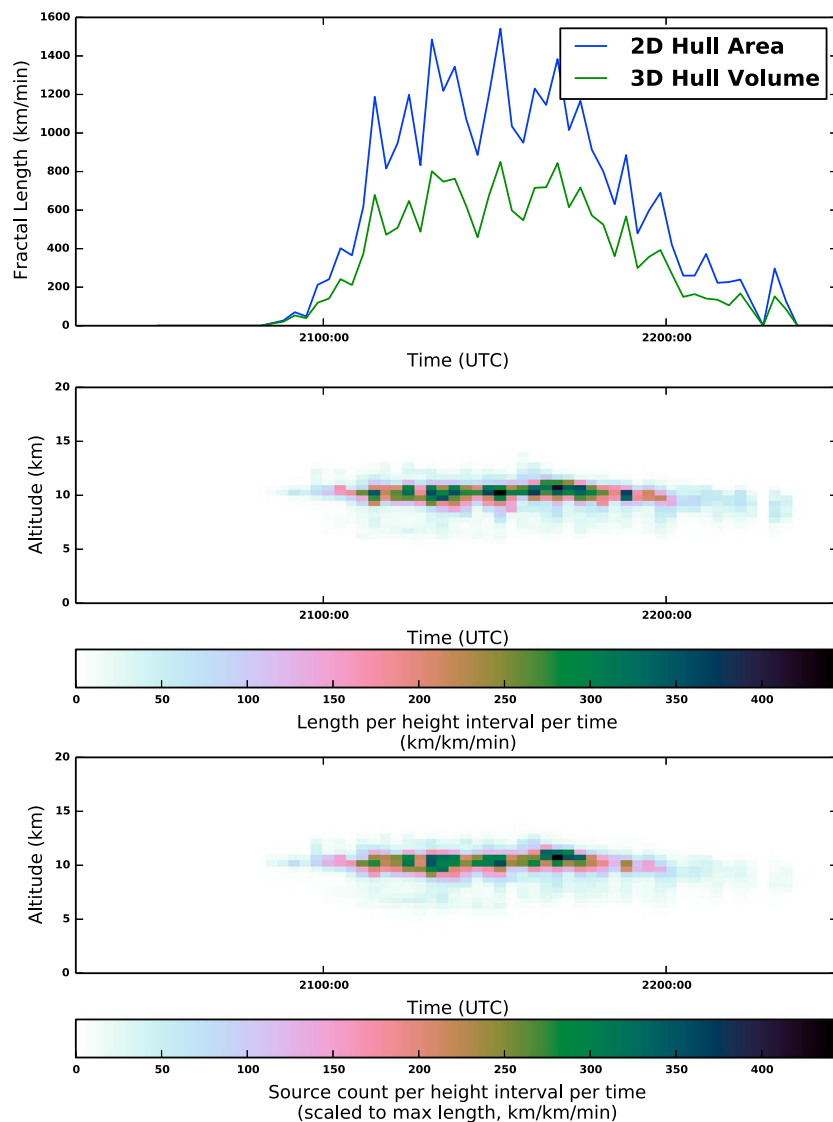


Figure 6. (top) Total flash length per minute, calculated using the fractal length method from the convex hull area and volume. (middle) Vertical distribution of channel length using the subvolume-weighting method. (bottom) VHF source density scaled to the maximum channel length in Figure 6 (middle).

flash rate decreased but more slowly than flash energy, which suggests that energy separated in storms' prior charging was dissipated in a time-lagged fashion, similar to the continuation of precipitation after strong updraft motions have ceased during a cell's decay stage.

The total length was estimated using both the 2-D and 3-D convex hulls of each flash (Figure 6). The flash length estimates varied by a factor of 2, as in the single-flash sensitivity study, but both show the same trends. The 3-D hull is more faithful to the actual geometry of the flash, which is not actually restricted in an infinitely thin plane. However, many flashes exhibit some layering, and the large gaps between the layers, which are included in the global convex hull volume, should not be filled with channel. A suggested approach for future work would be to split the flash into an upper and lower half and use the fractal approach to fill the convex hull volume for each polarity of channel, which would also permit use of a different D for each half [Williams, 2006; Warner *et al.*, 2012, 2013]. A degraded version of this approach would be to double the length calculated from the 2-D hull area.

Because both the $D \approx 1.5$ th moment and the second moment incorporate the other, lower order integer raw moments, the trend in the total length appears most similar to the total energy plot. As with the comparison

of the subvolume partition of flash length to source density, the time series of the storm total vertical distributions of length and source density are nearly identical.

5. Concluding Remarks

In this study, a flash size scale defined from the flash area has been demonstrated to be a particularly well-behaved LMA measurable. Flash length determined from the VHF source level data varies with the number of contributing stations and χ^2 . The fractal estimate of length determined from flash area does not vary as much with respect to these detection performance characteristics. The flash volume is also better behaved than a connect-the-dots approach, though it is more susceptible to outlier-type altitude errors.

Another way of viewing improved network performance, then, is to say that better performing LMAs keep filling in the region inside the convex hull and increase the length of the channel directly measured. Our analysis indicated that it was not clear where one should begin distinguishing the main channel from the side branches, nor was there any objective way to distinguish a breakpoint where the removal of false or noisy locations stopped and the removal of real points began—they appeared to blend smoothly into one another. On the other hand, the area decreased as noise was removed and became nearly constant beyond some quality threshold, helping to distinguish where noise ceased to influence the estimates.

Furthermore, using fractal geometric principles captures the tortuosity of the channel, including tortuosity not necessarily resolved by all LMA systems. The estimates remain bounded by imposition of a channel step length that acts as a fine-scale bound to the tortuosity. The tortuosity and step length have physical relevance because they are geometric properties that try to summarize the result of the underlying breakdown physics.

The area of the flash's convex hull is proportional to flash energy, and by using moments of the flash size distribution it is shown how the size scale determined from the flash area relates to energy. Therefore, the approach presented herein suggests a statistically well-founded way to mine lightning data for time-trending signals beyond those available from simply counting flashes. Flash rate trends are more variable but are balanced by variations in flash size so that the energy trend, which combines the zeroth through second standard moments, is smooth. Total channel length is a fractional moment between the first and second standard moments and varied more like total energy than flash rate.

The range of moments considered here encompasses many of the whole-flash properties with physical relevance and shows one way they can be determined from VHF LMA data. Much as a river network reflects extent and carrying capacity for drainage on the Earth's surface, the branched channels seen in the LMA data respond to the net electrostatic conditions within which other energy transfer processes take place. While the LMA-indicated channel formation process is only one part of the energy budget, it delineates a fundamental part of the charge transfer network that leads to other energy-dissipating processes such as light, heat, chemical reactions, and sound.

The methodology presented in this study is of particular relevance to lightning NO_x studies, because it provides quantitative trends of flash rate, channel length, and energy, all quantities hypothesized to correlate to NO_x production. By comparing NO_x measurements with these lightning parameters, it should be possible to test the hypotheses for NO_x production and reduce the scatter in the NO_x production estimates from lightning observations. There remains the need for estimates of NO_x production in atmospheric chemistry models, where flash rate is usually parameterized on precipitation, microphysical, or kinematic fields, and some mean NO_x per flash is assumed. This study has demonstrated that there is additional information in the flash size distribution and that consideration of this information gives a different but complementary time series trend in the lightning activity. Incorporation of variability in average flash size may better constrain these parameterizations of NO_x production.

Beirle et al. [2014] has examined flash size and radiance (a different energetic measure) for optical pulses detected by the space-based Optical Transient Detector and Lightning Imaging Sensor instruments. They found spatial variation in these properties, both within continents and between land and ocean. A future comparison of LMA and optical flash size and energy properties (especially with the upcoming GOES-R Geostationary Lightning Mapper) might reveal something about how energy is partitioned between leader development and stroke processes. Another global application of lightning energetics is found in *Romps et al.* [2014], who used an estimate of the energy per flash to predict lightning rate as a function of convective available potential energy and precipitation rate from climate model projections under climate change. The

regional variability noted by *Beirle et al.* [2014] and the DC3 observations suggests that regional variability of energy per flash should be incorporated into these large-scale studies.

Appendix A: Total Available Energy

Bruning and MacGorman [2013] found a predictable shape of the flash energy spectrum versus flash size $l = \sqrt{A_h}$. The total flash energy is related to the distribution of flashes at size l as follows.

$$E(l) = \frac{\rho^2 l^2 d^3}{2\epsilon_0} = Kl^2 \quad (\text{A1})$$

$$N(l) = N_T \int_0^\infty P(l) dl \quad (\text{A2})$$

$$E_T = \int_0^\infty E(l)N(l) dl \quad (\text{A3})$$

$$= KN_T \int_0^\infty l^2 P(l) dl, \quad (\text{A4})$$

where N_T is the total number of flashes and $P(l)$ is the probability density function for flash size. The total energy E_T over the collection of all flashes is the second raw moment of the flash size distribution. The $\epsilon_0 = 8.854 \times 10^{-12} \text{ F m}^{-1}$ is the electric permittivity. K is treated as a constant in this study and has units of kg s^{-2} . Variations in charge density ρ and spacing between the charge regions d could also be important, but we leave their study to future work, focusing here only on the dependence of energy on l . For $\rho = 0.5 \text{ nC m}^{-3}$ and $d = 1 \text{ km}$, $K \simeq 10 \text{ kg s}^{-2}$.

Leaving aside for now the shape and skew of the flash size distribution, it is helpful to assume several different distributions and look at the resulting formula for total energy. For normally distributed flash sizes with mean flash size μ and variance σ^2 ,

$$E_T = \frac{\rho^2 d^3}{2\epsilon_0} N_T (\mu^2 + \sigma^2). \quad (\text{A5})$$

For a lognormal distribution, with characteristic length scale $l_M = e^M$

$$N(l) = \frac{N_T}{S\sqrt{2\pi}l} \exp\left(-\frac{(\ln(l) - M)^2}{2S^2}\right) \quad (\text{A6})$$

$$E_T = \frac{\rho^2 d^3}{2\epsilon_0} N_T \exp(2(M + S^2)) \quad (\text{A7})$$

$$= \frac{\rho^2 d^3}{2\epsilon_0} N_T l_M^2 \exp(2S^2). \quad (\text{A8})$$

For a gamma distribution, with characteristic length scale θ ,

$$N(l) = N_T \frac{l^{\alpha-1} e^{-l/\theta}}{\Gamma(\alpha)\theta^\alpha} \quad (\text{A9})$$

$$E_T = \frac{\rho^2 d^3}{2\epsilon_0} N_T \theta^2 \frac{\Gamma(\alpha + 2)}{\Gamma(\alpha)} \quad (\text{A10})$$

For each distribution, there is a linear dependence on the product of the total flash rate and the “area” determined from the characteristic length scale of the distribution of flash sizes. There is also a dependence on the spread of the distribution, given by σ^2 , S^2 , and $\alpha + 2$ for the normal, lognormal, and gamma distributions, respectively.

Therefore, to the extent that flash energy variability is important, it is necessary to consider at least the zeroth through second moments of the flash size distribution. Furthermore, calculation of these additional moments provides flexibility when seeking to test the relationship of lightning to other properties of the thunderstorm, including NO_x production.

Appendix B: Relationship of Total Length to the Continuous Flash Size Distribution

For fractal dimension D , the total length is the D th moment of the size distribution. The relevant equations for single-flash length $L(l)$ and total length L_T are

$$L(l) = \frac{l^D}{b_s^{D-1}} \quad (\text{B1})$$

$$L_T = \int_{b_s}^{\infty} L(l)N(l)dl \quad (\text{B2})$$

$$= \frac{1}{b_s^{D-1}} \int_{b_s}^{\infty} l^D N(l)dl \quad (\text{B3})$$

$$= \frac{N_T}{b_s^{D-1}} \int_{b_s}^{\infty} l^D P(l)dl. \quad (\text{B4})$$

The total length integral is nontrivial in terms of the standard moment generating function, which is for integer values of the moment. The integral can be treated by application of fractional integration and differentiation, as in *Wolfe* [1975] who shows (p. 313) that this integral evaluates for a lower limit of integration of zero to infinity for all $D > 1$ as it should for a fractal. Recent work [*Cottone and Di Paola, 2009; Haeri and Shrimpton, 2012*] has made further progress in approximating this integral by Taylor series expansion. Their formulae are likewise for integration from zero, so a change of variable to adjust the lower limit of integration to b_s would be necessary to apply the above formulae. We suspect this will allow the integral to converge (as it did, empirically, above), though this activity is left for future work.

Appendix C: Time Series Statistics of the Flash Size Distribution

Statistics of the flash size distribution may be calculated from observed flash size data where l_j is known for each flash j over some duration (typically 1–2min is sufficient). The sample raw moments of the flash size distribution were calculated as follows. The notation is that of *Weisstein* [2014].

$$M_{i=0..4}^* = \sum_j l_j^i, \quad (\text{C1})$$

$$M_{i=1..4} = M_i^* / M_0^*. \quad (\text{C2})$$

Then the central moments were defined as

$$\mu_2 = M_2 - M_1^2, \quad (\text{C3})$$

$$\mu_3 = 2M_1^3 - 3M_1M_2 + M_3, \quad (\text{C4})$$

$$\mu_4 = -3 * M_1^4 + 6M_1^2M_2 - 4M_3M_1 + M_4, \quad (\text{C5})$$

so that the standard moments are given by

$$N_T = M_0^*, \quad (\text{C6})$$

$$\mu = M_1, \quad (\text{C7})$$

$$\sigma^2 = \mu_2, \quad (\text{C8})$$

$$\gamma_s = \mu_3 / \mu_2^{1.5}, \quad (\text{C9})$$

$$\gamma_k = \mu_4 / \mu_2^2 - 3, \quad (\text{C10})$$

where γ_s and γ_k are the skewness and kurtosis, respectively. The skewness and kurtosis were defined so that their values were zero for a normal distribution. Finally, the energy was calculated as

$$E_T/K = N_T(\mu^2 + \sigma^2). \quad (C11)$$

The form of equation (C11) matches that for the energy estimate for the normal distribution (equation (A5)). It is easily shown that

$$E_T/K = N_T M_2 = \sum_j I_j^2 = \sum_j (A_n)_j, \quad (C12)$$

i.e., the total energy is proportional to the simple sum of the areas of each flash, as in *Bruning and MacGorman* [2013]. Therefore, while thunderstorm flash size distributions typically exhibit some departure from a normal distribution, the estimate of energy from the mean and variance of the flash size distribution results in an estimate that exactly matches a direct sum of the discrete areas. In fact, we fitted flash size data to lognormal and gamma distributions, and total energy calculated from using equations (5)–(10) and the fit parameters always showed some differences relative to the direct, discrete method, suggesting that the fitting step is an unnecessary distraction from the objectives of this study.

References

Acknowledgments

The Deep Convective Clouds and Chemistry Experiment (DC3) is sponsored by the US National Science Foundation (NSF), the National Aeronautics and Space Administration (NASA), the National Oceanic and Atmospheric Administration (NOAA), and the Deutsches Zentrum für Luft- und Raumfahrt (DLR). This investigation was supported by NSF-1063966. The authors wish to acknowledge the rest of the Pls in the Colorado domain for availability of data during DC3. Data used in this study may be downloaded from the DC3 data archive at http://data.eol.ucar.edu/master_list/?project=DC3. We are grateful for the astute remarks of the reviewers of this study. These helped us clarify our findings.

- Allen, B., E. R. Mansell, and E. C. Bruning (2011), Fractal characteristics of simulated and LMA-detected lightning flashes, paper presented at Fifth Conference on Meteorological Applications of Lightning Data, Am. Meteorol. Soc. Seattle, 308 pp., Wash.
- Barth, M., et al. (2015), The Deep Convective Clouds and Chemistry (DC3) field campaign, *Bull. Am. Meteorol. Soc.*, doi:10.1175/BAMS-D-13-00290.1.
- Barthe, C., and M. C. Barth (2008), Evaluation of a new lightning-produced NO_x parameterization for cloud resolving models and its associated uncertainties, *Atmos. Chem. Phys.*, *8*, 4691–4710.
- Behnke, S. A., and E. C. Bruning (2015), Changes to the turbulent kinematics of a volcanic plume inferred from lightning data, *Geophys. Res. Lett.*, *42*, 4232–4239, doi:10.1002/2015GL064199.
- Beirle, S., W. Koshak, R. Blakeslee, and T. Wagner (2014), Global patterns of lightning properties derived by OTD and LIS, *Nat. Hazards Earth Syst. Sci.*, *14*(10), 2715–2726, doi:10.5194/nhess-14-2715-2014.
- Bruning, E. C., and D. R. MacGorman (2013), Theory and observations of controls on lightning flash size spectra, *J. Atmos. Sci.*, *70*(12), 4012–4029, doi:10.1175/JAS-D-12-0289.1.
- Bruning, E. C., W. D. Rust, T. J. Schuur, D. R. MacGorman, P. R. Krehbiel, and W. Rison (2007), Electrical and polarimetric radar observations of a multicell storm in TELEX, *Mon. Weather Rev.*, *135*(7), 2525–2544, doi:10.1175/MWR3421.1.
- Cooray, V., M. Rahman, and V. Rakov (2009), On the NO_x production by laboratory electrical discharges and lightning, *J. Atmos. Sol. Terr. Phys.*, *71*(17–18), 1877–1889, doi:10.1016/j.jastp.2009.07.009.
- Cottone, G., and M. Di Paola (2009), On the use of fractional calculus for the probabilistic characterization of random variables, *Probab. Eng. Mech.*, *24*(3), 321–330, doi:10.1016/j.probenmech.2008.08.002.
- DeCaria, A. J., K. E. Pickering, G. L. Stenchikov, J. R. Scala, J. L. Stith, J. E. Dye, B. Ridley, and P. Laroche (2000), A cloud-scale model study of lightning-generated NO_x in an individual thunderstorm during STERAO-A, *J. Geophys. Res.*, *105*, 11,601–11,616.
- DeCaria, A. J., K. E. Pickering, G. L. Stenchikov, and L. E. Ott (2005), Lightning-generated NO_x and its impact on tropospheric ozone production: A three-dimensional modeling study of a Stratosphere-Troposphere Experiment: Radiation, Aerosols and Ozone (STERAO-A) thunderstorm, *J. Geophys. Res.*, *110*, D14303, doi:10.1029/2004JD005556.
- Defer, E., P. Blanchet, C. Théry, P. Laroche, J. E. Dye, M. Venticinque, and K. L. Cummins (2001), Lightning activity for the July 10, 1996, storm during the Stratosphere-Troposphere Experiment: Radiation, Aerosol, and Ozone-A (STERAO-A) experiment, *J. Geophys. Res.*, *106*(D10), 10,151–10,172, doi:10.1029/2000JD900849.
- Defer, E., P. Laroche, J. Dye, and W. Skamarock (2003), Use of total lightning lengths to estimate NO_x production in a Colorado thunderstorm, paper presented at 12th International Conference on Atmospheric Electricity, Versailles, France.
- Ebert, U., C. Montijn, T. M. P. Briels, W. Hundsdorfer, B. Meulenbroek, A. Rocco, and E. M. V. Veldhuizen (2006), The multiscale nature of streamers, *Plasma Sources Sci. Technol.*, *15*(2), S118–S129, doi:10.1088/0963-0252/15/2/s14.
- Edens, H. E., K. B. Eack, W. Rison, and S. J. Hunyady (2014), Photographic observations of streamers and steps in a cloud-to-air negative leader, *Geophys. Res. Lett.*, *41*, 1336–1342, doi:10.1002/2013gl059180.
- Gallardo, L., and V. Cooray (1996), Could cloud-to-cloud discharges be as effective as cloud-to-ground discharges in producing NO_x ?, *Tellus B*, *48*, 641–651.
- Garik, P., K. Mullen, and R. Richter (1987), Models of controlled aggregation, *Phys. Rev. A*, *35*(7), 3046–3055, doi:10.1103/PhysRevA.35.3046.
- Haeri, S., and J. Shrimpton (2012), Closure of non-integer moments arising in multiphase flow phenomena, *Chem. Eng. Sci.*, *75*, 424–434, doi:10.1016/j.ces.2012.03.052.
- Hansen, A. E., H. E. Fuelberg, and K. E. Pickering (2010), Vertical distributions of lightning sources and flashes over Kennedy Space Center, Florida, *J. Geophys. Res.*, *115*, D14203, doi:10.1029/2009JD013143.
- Ivezić, Ž., A. J. Connolly, J. T. VanderPlas, and A. Gray (2014), *Statistics, Data Mining, and Machine Learning in Astronomy: A Practical Python Guide for the Analysis of Survey Data*, Princeton Univ. Press, Princeton, N. J.
- Kitagawa, N., and M. Brook (1960), A comparison of intracloud and cloud-to-ground lightning discharges, *J. Geophys. Res.*, *65*(4), 1189–1201, doi:10.1029/JZ065i004p01189.
- Koshak, W., and H. Peterson (2011), A summary of the NASA Lightning Nitrogen Oxides Model (LNOM) and recent results, paper presented at 10th Annual Community Modeling and Analysis System (CMAS) Conference, Chapel Hill, NC. Preprints.
- Koshak, W., H. Peterson, A. Biazar, M. Khan, and L. Wang (2014), The NASA Lightning Nitrogen Oxides Model (LNOM): Application to air quality modeling, *Atmos. Res.*, *135*, 363–369, doi:10.1016/j.atmosres.2012.12.015.
- Koshak, W. J., H. S. Peterson, E. W. McCaul, and A. Biazar (2010), Estimates of the lightning NO_x profile in the vicinity of the North Alabama Lightning Mapping Array, paper presented at 3rd International Lightning Meteorology Conference, Tuscon, AZ, Vaisala, 19–20 April 2010.

- Koshak, W. J., R. J. Solakiewicz, and H. S. Peterson (2015), A return stroke NO_x production model, *J. Atmos. Sci.*, *72*(2), 943–954, doi:10.1175/jas-d-14-0121.1.
- Liaskos, C. E., D. J. Allen, and K. E. Pickering (2015), Sensitivity of tropical tropospheric composition to lightning NO_x production as determined by the NASA GEOS-Replay model, *J. Geophys. Res. Atmos.*, *120*, doi:10.1002/2014JD022987.
- McCaul, E. W., S. J. Goodman, K. M. LaCasse, and D. J. Cecil (2009), Forecasting lightning threat using cloud-resolving model simulations, *Weather Forecasting*, *24*(3), 709–729, doi:10.1175/2008WAF2222152.1.
- Mecikalski, R. M., A. L. Bain, and L. D. Carey (2015), Radar and lightning observations of deep moist convection across northern Alabama during DC3: 21 May 2012, *Mon. Weather Rev.*, *143*(7), 2774–2794, doi:10.1175/MWR-D-14-00250.1.
- Niemeyer, L., L. Pietronero, and H. J. Wiesmann (1984), Fractal dimension of dielectric breakdown, *Phys. Rev. Lett.*, *52*, 1033–1036.
- Nijdam, S., E. M. van Veldhuizen, and U. Ebert (2010), Comment on “ NO_x production in laboratory discharges simulating blue jets and red sprites” by H. Peterson et al., *J. Geophys. Res.*, *115*, A12305, doi:10.1029/2010JA015861.
- Normant, F., and C. Tricot (1991), Method for evaluating the fractal dimension of curves using convex hulls, *Phys. Rev. A*, *43*(12), 6518–6525.
- Ott, L. E., K. E. Pickering, G. L. Stenichkov, D. J. Allen, A. J. DeCaria, B. Ridley, R.-F. Lin, S. Lang, and W.-K. Tao (2010), Production of lightning NO_x and its vertical distribution calculated from three-dimensional cloud-scale chemical transport model simulations, *J. Geophys. Res.*, *115*, D04301, doi:10.1029/2009JD011880.
- Price, C., and D. Rind (1992), A simple lightning parameterization for calculating global lightning distributions, *J. Geophys. Res.*, *97*, 9919–9933, doi:10.1029/92JD00719.
- Ridley, B. A., K. E. Pickering, and J. E. Dye (2005), Comments on the parameterization of lightning-produced NO in global chemistry-transport models, *Atmos. Environ.*, *39*(33), 6184–6187, doi:10.1016/j.atmosenv.2005.06.054.
- Riousset, J. A., V. P. Pasko, P. R. Krehbiel, R. J. Thomas, and W. Rison (2007), Three-dimensional fractal modeling of intracloud lightning discharge in a New Mexico thunderstorm and comparison with lightning mapping observations, *J. Geophys. Res.*, *112*, D15203, doi:10.1029/2006JD007621.
- Rison, W., R. J. Thomas, P. R. Krehbiel, T. Hamlin, and J. Harlin (1999), A GPS-based three-dimensional lightning mapping system: Initial observations in central New Mexico, *Geophys. Res. Lett.*, *26*, 3573–3576.
- Romps, D. M., J. T. Seeley, D. Vollaro, and J. Molinari (2014), Projected increase in lightning strikes in the United States due to global warming, *Science*, *346*(6211), 851–854, doi:10.1126/science.1259100.
- Sañudo, J., J. B. Gómez, F. Castaño, and A. F. Pacheco (1995), Fractal dimension of lightning discharge, *Nonlinear Processes Geophys.*, *2*, 101–106.
- Schumann, U., and H. Huntrieser (2007), The global lightning-induced nitrogen oxides source, *Atmos. Chem. Phys.*, *7*, 3823–3907.
- Skamarock, W. C., J. E. Dye, E. Defer, M. C. Barth, J. L. Stith, B. A. Ridley, and K. Baumann (2003), Observational- and modeling-based budget of lightning-produced NO_x in a continental thunderstorm, *J. Geophys. Res.*, *108*(D10), 4305, doi:10.1029/2002JD002163.
- Theiler, J. (1990), Estimating fractal dimension, *J. Opt. Soc. Am. A*, *7*(6), 1055–1073.
- Thomas, R. J., P. R. Krehbiel, W. Rison, S. J. Hunyady, W. P. Winn, T. Hamlin, and J. Harlin (2004), Accuracy of the Lightning Mapping Array, *J. Geophys. Res.*, *109*, D14207, doi:10.1029/2004JD004549.
- Tsonis, A. A. (1991), A fractal study of dielectric breakdown in the atmosphere, in *Non-Linear Variability in Geophysics*, edited by D. Schertzer and S. Lovejoy, pp. 167–174, Springer, Netherlands, doi:10.1007/978-94-009-2147-4_11
- Vecchi, G., D. Labate, and F. Canavero (1994), Fractal approach to lightning radiation on a tortuous channel, *Radio Sci.*, *29*(4), 691–704, doi:10.1029/93RS03030.
- Wang, Y., A. W. DeSilva, G. C. Goldenbaum, and R. R. Dickerson (1998), Nitric oxide production by simulated lightning: Dependence on current, energy, and pressure, *J. Geophys. Res.*, *103*(D15), 19,149–19,159, doi:10.1029/98JD01356.
- Warner, T. A., K. L. Cummins, and R. E. Orville (2012), Upward lightning observations from towers in Rapid City, South Dakota and comparison with National Lightning Detection Network data, 2004–2010, *J. Geophys. Res.*, *117*, D19109, doi:10.1029/2012JD018346.
- Warner, T. A., M. M. F. Saba, R. E. Orville, K. L. Cummins, and W. A. Lyons (2013), Differences in positive and negative lightning leader appearance and behavior as observed by high-speed cameras, paper presented at Sixth Conference on the Meteorological Applications of Lightning Data, AMS Annual Meeting, Austin, Tex.
- Weisstein, E. W. (2014), Moment. From *MathWorld*—A Wolfram Web Resource. [Available at <http://mathworld.wolfram.com/Moment.html>.]
- Williams, E. R. (2006), Problems in lightning physics—The role of polarity asymmetry, *Plasma Sources Sci. Technol.*, *15*(2), 91–108, doi:10.1088/0963-0252/15/2/S12.
- Winn, W. P., G. D. Aulich, S. J. Hunyady, K. B. Eack, H. E. Edens, P. R. Krehbiel, W. Rison, and R. G. Sonnenfeld (2011), Lightning leader stepping, K changes, and other observations near an intracloud flash, *J. Geophys. Res.*, *116*, D23115, doi:10.1029/2011JD015998.
- Wolfe, S. (1975), On moments of probability distribution function, in *Fractional Calculus and Its Applications: Proceedings of the International Conference Held at the University of New Haven, June, 1974, Lect. Notes Math.*, vol. 457, edited by B. Ross, pp. 306–316, Springer, Berlin, New York.